Reviving the Absorbent Chemistry of Electrochemically Mediated Amine Regeneration for Improved Point Source Carbon Capture

Ahmad Hassan[1], Abdelrahman Refaie[1], Prince Aleta[1], Mohsen Afshari[1], Elmira Kalantari[1], Yuanyuan Fang[1], M. Mim Rahimi[1,2,*]

[1] Department of Civil and Environmental Engineering, University of Houston, Houston, TX 77204, USA
[2] Materials Science and Engineering Program, University of Houston, Houston, TX 77204, USA
* Corresponding Author: mrahimi@uh.edu

GRAPHICAL ABSTRACT

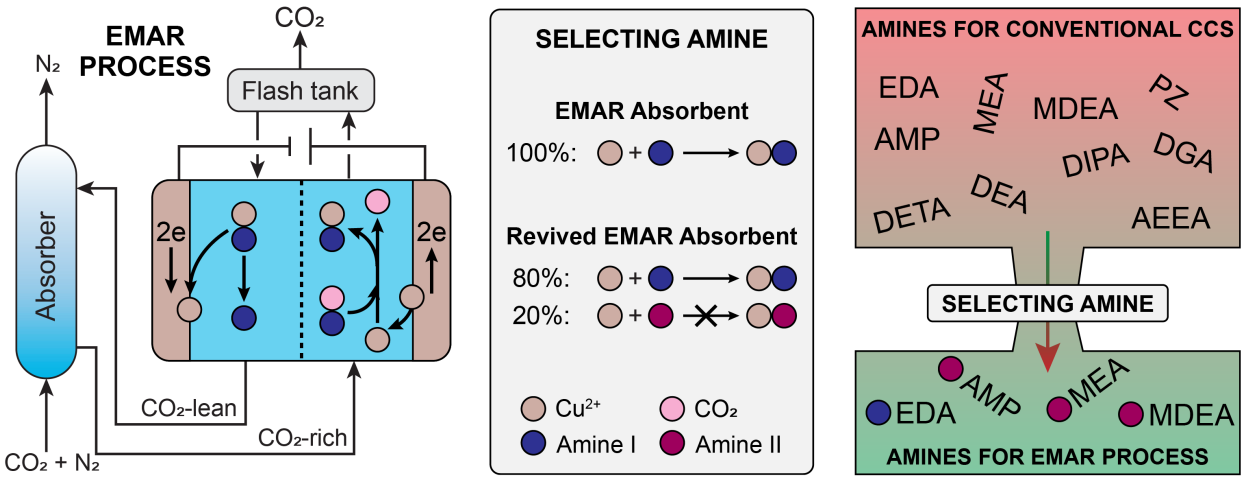

ABSTRACT

Electrochemically mediated amine regeneration (EMAR) is emerging as a promising electrochemical approach for carbon capture from point sources. In this study, for the first time, the absorbent chemistry of the EMAR process was revived by considering criteria beyond metal-amine complexation. The systematic investigation focused on using secondary amines, which were previously overlooked in EMAR due to limited metal-amine interaction, despite their proven effectiveness in conventional carbon capture processes. The integration of secondary amines—monoethanolamine (MEA), aminomethyl propanol (AMP), and methyldiethanolamine (MDEA)—with the benchmark ethylenediamine (EDA) was thoroughly studied, evaluating their impact on absorption and desorption kinetics and capacities, and electrochemical performance. Among the blends, EDA+MDEA emerged as the top performer, particularly excelling in electrochemical aspects. The charge transfer resistance (R_{CT}) of the deposition reaction, as the rate-limiting step, for the EDA+MDEA blend was reduced by 40% compared to pure EDA, and the heterogeneous electron transfer rate constant (k^0) improved threefold. In the bench-scale assessments, the EDA+MDEA blend showed a notable decrease in desorption energetics to 37 kJ/molCO_2, marking a 34% reduction compared to the 56 kJ/molCO_2 required for pure EDA. This marks the lowest reported energetics for an EMAR process targeting point source carbon capture. This research paves the way for future systematic investigations of a wider range of amine blends for EMAR and eventually the process implementation at larger scales.

Keywords: Climate Change, Carbon Capture, Electrochemical Processes, EMAR, Amine Blend

1 INTRODUCTION

Among all greenhouse gas emissions, the anthropogenic rise in atmospheric carbon dioxide (CO_2) since the beginning of the industrial age stands widely acknowledged as the primary driver of climate change, necessitating effective action to combat its impact on the environment [1-4]. In response to this urgency, the Intergovernmental Panel on Climate Change (IPCC) has put forth scenarios aimed at limiting the average temperature increase to below 2°C by the end of this century, primarily through the reduction of CO_2 emissions [1]. To achieve this goal, two primary strategies have been proposed: complete reliance on renewables (decarbonization) and the utilization of fossil fuels with carbon capture and storage (CCS), either independently or in combination [5]. However, the considerable energy demand and the availability of cheaper fossil fuels have slowed down the decarbonization process [5, 6]. Consequently, alongside exploring other sustainable approaches to limit global temperature rise, the deployment of CCS on major point source emitters, particularly electricity generation, becomes imperative [7].

The state-of-the-art technology for carbon capture from point sources, commonly known as thermal amine scrubbing, involves nucleophilic solvents that absorb CO_2 from flue gases followed by regeneration through the thermal swing process [7-9]. Although amine absorbents offer high absorption capacity and fast kinetics for CO_2 capture [10-13], the thermal nature of the amine scrubbing process presents practical challenges when deployed commercially. This includes issues such as amine degradation and high energetics, owing to the substantial heat requirement for the regeneration of the saturated solvent at elevated temperatures (100-140°C) [14-16]. Ongoing efforts are being made to address these challenges and improve the process's overall efficiency and sustainability.

In this context, electrochemical carbon capture (ECC) technologies are emerging as a valuable addition to the conventional thermal amine process offering solutions to the technological challenges outlined. ECCs are in general less energy-intensive and hold the promise of operating with a minimal carbon footprint when exclusively powered by renewable sources [3, 17, 18]. Additionally, the ease of scalability, plug-and-play nature of operation, and lower regeneration temperature requirements not only promise seamless adoption but also contribute to reduced operational costs by mitigating concerns regarding solvent losses [19, 20].

The evolving field of ECC can be categorized into four main branches depending on the mechanism they follow to separate CO_2 from a gas mixture: (1) electrochemical generation of nucleophiles (EGN) [21-23], (2) electrochemical modulation of proton concentration (EMPC)

commonly known as pH swing [24-27], (3) electrochemical capacitive adsorption (ECA) [28-30], and (4) electrochemically mediated amine regeneration (EMAR) [3, 19, 31, 32]. Other emerging ECC processes, recently introduced, also follow systematic mechanisms for carbon capture [33-35]. Among these outlined ECC approaches, EMAR has achieved developments at larger scales. While other methods are primarily developed on a small scale and tested for limited regeneration cycles, EMAR's experimental setup has expanded beyond that, having been operated continuously for over 100 hours using a fully automated lab-scale system [19]. This progress is partly attributed to EMAR being inspired by conventional processes, allowing expertise developed over the past fifty years to be directly applied to EMAR. Another factor contributing to EMAR's success is its robustness in various operational conditions. For instance, unlike the EGN process that uses quinone as redox-active molecules, suffering from performance issues in the presence of oxygen in the input gas stream [36], EMAR generally maintains its performance even in the presence of oxygen [19, 37]. These advantages have pushed EMAR to gain momentum in current research trends [3, 32, 38-40], positioning it as an efficient and scalable solution for carbon capture.

An EMAR cycle includes two stages: (1) chemical absorption of CO_2 from the gas stream using an amine absorbent, and (2) electrochemical CO_2 desorption followed by absorbent regeneration. The absorption step resembles the thermal amine process, where the solvent comes into contact with CO_2 in the absorber column. However, the key difference lies in the regeneration of the solvent, which takes place in an electrochemical cell featuring two compartments: the anode and the cathode. For the desorption of CO_2, the EMAR employs a metal electrode that is present as an active anode and cathode in the cell. Following the absorption of the gas, the CO_2-rich solvent is directed to the anode chamber, where the active metal electrode undergoes oxidation, releasing metal cations into the solution ($M \rightarrow M^{n+} + n\ e^-$). These cations have higher affinities to complex with the amine, resulting in the displacement of the CO_2 from the saturated stream ($M^{n+} + m$ amine-$CO_2 \rightarrow M(amine)_m^{n+} + m\ CO_2$). The desorbed CO_2 is removed via a flash tank installed after the anode compartment. The resulting cations-saturated solution is then transferred to the cathode chamber, where the metal ions are electroplated onto the cathode ($M(amine)_m^{n+} + n\ e^- \rightarrow M + m$ amine), enabling the efficient regeneration of the amine solution for subsequent cycles [19, 41].

The critical aspect in designing the EMAR process involves choosing a suitable combination of active metal and amine. The choice of metal relies on factors including its binding strength with the amine, chemical stability (e.g., the resistance against oxidation), cost, and availability.

Considering these factors, copper (Cu) is the most commonly chosen metal due to its favorable characteristics [19, 41, 42]. Besides factors such as rapid kinetics and adequate CO_2 loading capacity, the primary criterion for amine selection is its capacity to form stable metal ion complexes, which aids in CO_2 desorption while mitigating the risk of unwanted precipitation [41]. Therefore, many amines previously developed for conventional amine-based carbon capture, such as monoethanolamine (MEA), were found unsuitable for the EMAR cycle [41, 43]. Instead, a limited selection of amines, including ethylenediamine (EDA), aminoethyl ethanolamine (AEEA), diethylenetriamine (DETA), and triethylenetetramine (TETA), were identified and investigated for their compatibility with EMAR [19, 43, 44]. Among these options, EDA emerged as the most suitable choice due to its lower energetics for regeneration and formation of stable copper complexes [41, 45].

Recent models on the EMAR energetics have challenged the assumption that 100% of the amines should be electroactive, i.e., able to complex with copper ions. These models revealed that for the most energy-efficient operation, approximately 80% of the copper ions need to complex with the amine [31]. This opens up new possibilities to explore non-electroactive amines, which potentially can replace 20% of the electroactive amine (e.g., EDA), thereby offering a broader range of options for the new chemistry of EMAR absorbents.

In this study, for the first time, the absorbent chemistry of the EMAR process was revived by considering criteria beyond metal ion complexation. The use of secondary amines, previously overlooked due to their limited interaction with metal ions but known for their high performance in conventional carbon capture processes, was systematically investigated. Different amine blends were chosen, with EDA as the benchmark amine, which is the most commonly used electroactive amine in EMAR. Alongside EDA, three other amines were included mainly inspired by the conventional thermal amine processes. The first is MEA, a primary amine commonly used for its fast reaction kinetics with CO_2. The second is methyldiethanolamine (MDEA), a tertiary amine known for its excellent CO_2 absorption capacity. The third is aminomethyl propanol (AMP), a sterically hindered amine that has recently gained attention for its unique blend of high CO_2 absorption capacity and rapid kinetics. By blending MEA, MDEA, and AMP with EDA, we intend to revive the absorbent chemistry for improved carbon capture, utilizing their strengths to enhance the overall performance of the EMAR system. The blending approach has been extensively investigated in the conventional thermal amine processes and has demonstrated its effectiveness in achieving multiple objectives, including enhanced absorption capacity, cost reduction, and improved energetics [46, 47].

This investigation aimed to comprehensively explore the impact of a blend of amines on the absorption kinetics, absorption capacity, and electrochemical desorption performance in the EMAR system. The systematic assessments helped identify the amine blend that outperformed the benchmark EDA. The selected amine blend was then further evaluated in a lab-designed bench-scale EMAR cell to assess its overall performance in capturing CO_2 from simulated industrial flue gas.

2 MATERIALS AND METHODS

2.1 Electrolytes Preparation

Chemical solutions were prepared using deionized water with a resistivity greater than 18 MΩ·cm. The chemicals that were used in the experiments include copper (II) sulfate pentahydrate ($CuSO_4.5H_2O$; 98% purity, Sigma Aldrich), sodium sulfate (Na_2SO_4; purity >99.0%, Sigma Aldrich), EDA (Sigma Aldrich), MEA (Sigma Aldrich), MDEA (Sigma Aldrich) and AMP (Sigma Aldrich). Three blend samples were prepared, each consisting of 80% EDA and 20% of one of the secondary amines—either MEA, AMP, or MDEA. In each blend, the total amine concentration was maintained at 1 M, i.e., 0.8 M EDA and an additional 0.2 M of the secondary amine. Additionally, a reference sample containing 1 M EDA, labeled as pure EDA, was prepared to serve as a benchmark for comparison with the blend solutions. All four samples, including pure EDA, EDA+MEA, EDA+AMP, and EDA+MDEA, were supplemented with 0.25 M $CuSO_4$ as the initial source of cupric ions (Cu^{2+}) and 0.5 M Na_2SO_4 as a supporting electrolyte to enhance the overall electrochemical performance and the conductivity of the solutions.

2.2 CO_2 Absorption Kinetics and Capacity Measurement

A measured volume of 70 mL of Cu-amine solution comprising either pure EDA or three mixed amine samples was carefully transferred into a 100 mL three-neck round-bottom glass flask. The flask was precisely sealed with rubber corks on all openings to ensure a gas-tight setup. One neck of the flask was designated for the flue gas purging, featuring a gas diffuser submerged in the Cu-amine solution, while another neck housed a temperature probe (IKA; HS 90) to record any possible temperature fluctuations during the absorption process. The third neck at the center of the flask accommodated a condenser (IKA, RC2) maintained at a constant temperature of 5°C to facilitate the return of any evaporated water or amine to the flask. A mass flow controller (Masterflex; MFLX32907-59) was utilized to precisely blend individual gasses to generate a simulated flue gas stream and introduce a desirable flow rate of the generated gas into the

absorption flask. The gas exiting from the top of the condenser was further connected to an inline mass flowmeter (Alborg Digital Mass Flowmeter, XFM07) to accurately record the flow rate of the gas exiting the condenser over time. The composition of the gas was identified using a CO_2 infrared (IR) sensor (SpringIR; CM-20820) inserted after the mass flowmeter. The result always indicated no trace of water or the amines, confirming the effectiveness of the condenser. The electrolyte solution was continuously stirred at 400 RPM and kept at a constant temperature, either 25°C or 50°C, using a heating plate and stirrer (IKA; HS-90) (Figure 1A). The two temperatures were selected to assess the absorption performance of various electrolytes at ambient conditions and elevated temperatures representative of industrial flue gas (ranging from 40°C to 60°C). This selection provides critical data for future operations whether the process involves cooling the flue gas or operating the system at the flue gas temperature.

Once the setup was prepared, the amine solution was purged with the simulated industrial flue gas (15% CO_2, 7% O_2, and 78% N_2) for 100 minutes to evaluate the absorption kinetics of different samples. The amount of CO_2 absorbed in the solution was determined by subtracting the flow rate of the unabsorbed gas, as measured by the inline mass flowmeter, from the set input flow rate. Simultaneously, continuous temperature measurements were logged by the software (IKA; Labworldsoft6), aided by the temperature probe inserted into the solution. These temperature measurements helped with tracking the changes in temperature following the saturation of the solution with CO_2. The change in CO_2 absorption loading (defined as moles of CO_2 absorbed per 1 mole of amine) was determined by converting the mass flow rate of the absorbed CO_2 in the amine solution over time into the moles of CO_2.

2.3 Physiochemical Properties Measurements

Investigating the physicochemical properties, such as pH, conductivity, and viscosity, is crucial for understanding the impact of CO_2 absorption in the EMAR process. To understand the influence of CO_2 absorption on the pH and conductivity, we measured these parameters before and after CO_2 purging to realize if adjustments to the electrochemical process were necessary with blended absorbent solutions. These measurements were carried out using a multi-modular pH and conductivity meter (Mettler Toledo; S975) at both temperatures. Viscosity is a crucial property in the development of novel absorbent chemistries for carbon capture applications [48, 49], as high viscosities impose significant energy penalties for circulating the absorbent solution between the absorption column and the electrochemical cell. Hence, the viscosity of all absorbent solutions, both saturated and unsaturated, was carefully measured across a broad temperature spectrum using a viscometer (IKA; ROTAVISC lo-vi). The samples were filled into the assembly until the

spindle (IKA, SP1) was fully immersed in the solution. The temperature range for these viscosity measurements was expanded from 25°C to 75°C, using a circulating water bath provided by a heater (IKA; HRC 2 control).

Qualitative evaluation of sample saturation was conducted through Fourier Transform Infrared (FTIR) spectroscopy (Thermo Scientific; Nicolet iS5). This analytical method was employed to assess the molecular composition and structural changes after saturation of the samples with flue gas at ambient room temperature. The FTIR measurements were performed in absorbance mode, employing an Attenuated Total Reflection (ATR) setup utilizing a diamond crystal. The spectral analysis covered a wavenumber range spanning from 1000 cm^{-1} to 1800 cm^{-1} to capture the vibrational frequencies indicative of carbamate and bicarbonate functional groups.

2.4 CO_2 Desorption Kinetics

The desorption kinetics were quantified by simulating the anode reaction of the electrochemical cell, specifically the introduction of cupric ions through the oxidation of a copper anode. This was accomplished by initiating the desorption of a CO_2-loaded solution via the controlled addition of cupric ions, achieved by injecting 3 M $CuSO_4$ solution using a syringe pump (Pump Systems Inc.; NE-8000). The steady infusion of these

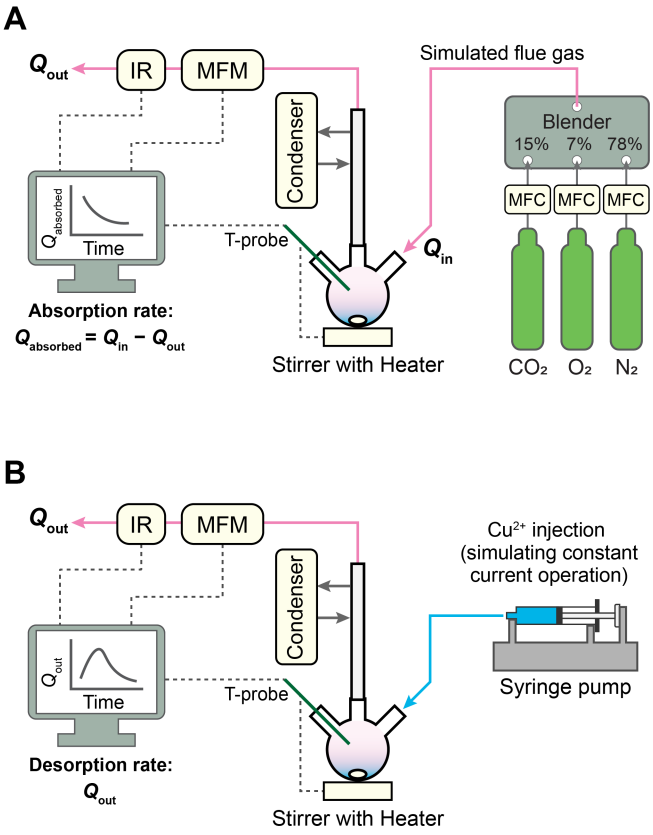

Figure 1. Schematics of the absorption and desorption experiments. (A) A three-neck round-bottom glass flask equipped with a condenser and temperature probe (T-probe) was used for the absorption experiments. Solutions were purged by simulated flue gases generated by precisely blending 15% CO_2, 7% O_2, and 78% N_2 using mass flow controllers (MFC). The gas exiting from the top of the condenser was further analyzed using an inline mass flowmeter (MFM) and infrared (IR) sensor. The amount of CO_2 absorbed in the solution ($Q_{absorbed}$) was determined by subtracting the flow rate of the unabsorbed gas (Q_{out}) from the set input flow rate (Q_{in}). (B) The same glass flask equipped with the condenser and temperature probe was used for the desorption experiments. Cupric ions (Cu^{2+}) were introduced to the desorption media using a syringe pump to represent the constant current operation. The output flow rate of CO_2 (Q_{out}) was continuously recorded to evaluate the desorption rate.

ions represented the constant current operation of an electrochemical cell. This was done for 20 minutes, maintaining a fixed injection flow rate of 2 mL/min. The gas-tight setup, initially employed for the CO_2 absorption experiment, was also used for the CO_2 desorption process, as illustrated in Figure 1B. The key difference was in measuring the gas flow rate during desorption, rather than the unabsorbed flow of CO_2 in the absorption experiment. The flow rate of CO_2 was continuously monitored with the same inline mass flowmeter until the meter readings reached zero, indicating complete desorption. To quantify the extent of desorption (total desorbed CO_2; %) specifically resulting from the introduction of Cu^{2+} in the solution, the difference in CO_2 loading was determined experimentally through the acid titration method, both before and after the desorption. The details of this acid titration experiment are described in the literature [19, 31]. Similar to the absorption experiments, desorption experiments were conducted at both temperatures, i.e., 25°C and 50°C.

2.5 Electrochemical Measurements

The fundamental electrochemical characteristics of the EMAR process using the tested absorbents were assessed through electrochemical impedance spectroscopy (EIS) and rotating disk electrode (RDE) techniques. EIS was used to evaluate distinct components of electrochemical resistance, including the solution resistance (R_S) and the charge transfer resistance of the redox reaction (R_{CT}). The EIS measurements were conducted using a custom-built EIS cell, wherein the working electrode (WE) comprised a copper mesh, and the counter electrode (CE) consisted of a platinum mesh. A reference electrode (RE; Ag/AgCl saturated with KCl) was positioned at the center of the cell. Both the anode and the cathode were of the same size (1.5 cm diameter), and the distance between them was fixed at 3 cm for consistent measurements. The WE was subjected to polarization at 0.1 V and −0.1 V versus the open circuit (OC) voltage to investigate the aforementioned resistance components during the corrosion and deposition processes, respectively. The EIS measurements were performed over a frequency range of 100 kHz to 100 Hz, utilizing a sinusoidal amplitude of 10 mV. To differentiate the resistance components, i.e., $R_{S,}$ and R_{CT}, the acquired EIS data were fitted to a Randles circuit model, which has been validated as a representative equivalent circuit for similar systems [37, 50, 51]. The EIS data were presented as Nyquist plots, which included the fitted model.

The RDE technique was utilized to gain a further understanding of the kinetics involved in the rate-determining step (deposition) by eliminating the mass transport limitations. A Levich study, a common experiment performed using RDE, was conducted to reveal the kinetic characteristics in the presence of different absorbent solutions. The Levich experiment was conducted using a

glassy carbon electrode, which was coated with an electrodeposited copper layer. This involved polarizing the electrode at −0.2 V vs. OC for 20 minutes. During this process, the electrode was rotated at a constant speed of 300 RPM in a 0.5 M $CuSO_4$ solution, ensuring a smooth deposition of Cu^{2+} from the bulk solution onto the glassy carbon electrode. The prepared Cu-coated glassy carbon electrode was then assembled in the RDE setup as a WE, alongside a RE (Ag/AgCl in saturated KCl) and a platinum wire CE. After transferring the saturated solution into the RDE cell, the experiment was initiated by performing cyclic voltammetry (CV) with an applied voltage range from −0.8 to 0.5 V vs. RE using a potentiostat (Biologic; VMP-300), while simultaneously rotating the electrode at controlled speeds of 400, 900, 1600, 2500, 3400, and 4900 RPM using a rotator (Biologic; BluRev Rotator). The response of the applied voltage was observed by recording the current at different applied rotational speeds. Finally, Levich analysis was conducted using the potentiostat built-in software (Biologic; EC-Lab). This analysis utilized input parameters such as viscosity, diffusion coefficient, area of the electrode, and the number of electron transfers for the deposition reaction to calculate the deposition heterogeneous electron transfer rate constant (k^0) in the presence of different absorbent samples. The data from the kinetically-controlled region of the Levich plot were fitted to estimate the rate constants.

2.6 Bench-Scale Demonstration

A flow-based electrochemical setup was developed to investigate the EMAR performance to capture CO_2 from simulated flue gas using developed absorbent solutions. The experiments were performed in a bench-scale apparatus specifically designed and fabricated in our lab. The cell comprised two chambers – a cathode and anode made of solid Cu plates– separated by an anion-exchange membrane (Fumasep FAS-PET-130,80µm). The projected surface area of the electrode after the incorporation of the acrylic baffles to create a flow path within the chambers was 50 cm^2. The entire cell was supported by high-density polyethylene (HDPE) housings (15x15 cm) on both sides, with two aluminum end plates on the outside to secure the entire cell structure. The anolyte and catholyte were circulated between the respective chambers and reservoir tanks by a peristaltic pump (Reglo Peristaltic Pump; Ismatec) with four independent controllable channels. The anolyte consisted of a Cu-amine solution saturated with a simulated flue gas (15% CO_2 7% O_2 and 78% N_2) and with a Cu loading (i.e., moles of Cu per 1 mole of amine) of 0.1, while the catholyte comprised a Cu-amine solution with a Cu loading of 0.4. The anolyte solution's composition represents the CO_2-rich stream exiting the absorption column in the integrated EMAR setup, while the catholyte's composition represents that of a CO_2-lean stream exiting the flash tank. The desorbed CO_2 from the anode side of the cell was removed from the anolyte tank, and the desorption rate was quantified using a subsequent gas flow meter and a CO_2 IR sensor.

Similar to the absorption experiment, a condenser was utilized to prevent potential evaporation of water and electrolyte. A schematic diagram and image of the bench-scale EMAR cell developed for studying the absorbents are shown in Figure 2. The developed bench-scale setup was employed to compare the energy requirements of carbon capture using various absorbent solutions. Chronopotentiometry experiments, operating at a constant current of 0.5 A for 80 minutes, were conducted to ensure the desired swing in the Cu loading of the anolyte between 0.1 and 0.4. During the experiment, the cell potential and CO_2 desorption profile were monitored to calculate the desorption energy (W; kJ/molCO_2):

$$W = \frac{\int_0^{t_0} UIdt}{\Delta n_{CO_2}} \qquad (1)$$

where U (V) and I (A) respectively represent the voltage and current, and Δn_{CO_2}(mol) denotes the number of moles of CO_2 desorbed from time zero to t_0. The voltage response in the chronopotentiometry experiment was recorded by the potentiostat software (Biologic; EC-Lab), while the moles of CO_2 desorbed were measured experimentally using the acid titration method and gas flow meter data.

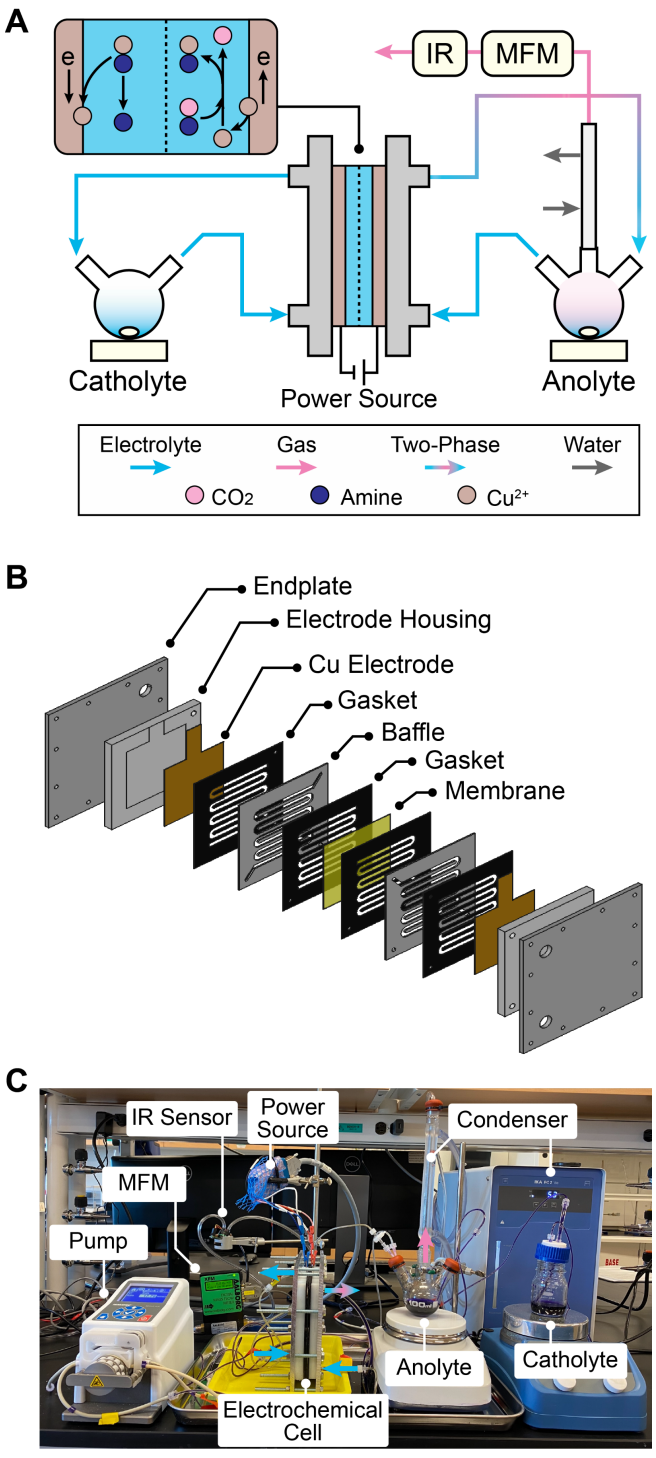

Figure 2. A bench-scale demonstration of EMAR. (A) A schematic illustration of the developed EMAR process to investigate different absorbents. The desorbed gas from the electrochemical cell was analyzed using a mass flowmeter (MFM) and CO_2 IR sensor. (B) A 3D schematic of the electrochemical cell with all the components. (C) A photograph of the developed experimental bench-scale setup.

3 RESULTS AND DISCUSSION

3.1 Absorption Kinetics and Capacity

CO_2 absorption kinetics and capacity are key factors in the design of novel amine absorbents for EMAR. In this context, EDA is largely acknowledged for its robust CO_2 absorption capacity and reasonable fast reaction kinetics [19, 37]. In developing a new blend of absorbent with EDA and the secondary amines, it becomes important to either preserve or improve the similar level of performance. Therefore, absorption kinetics and capacity were systematically evaluated utilizing the absorption setup described earlier. The results of the CO_2 absorption experiment are represented by the absorption profiles (change in flow rate of purged CO_2 over time) for all the samples at two temperatures, 25°C, and 50°C, in Figure 3. In all four samples, the flow rate of the absorbed CO_2 decreased over time until they reached their saturation where they no longer can absorb CO_2. However, the time interval to reach the saturation was different for all the samples because of its dependence on the reaction of amine with CO_2 in flue gas. To quantify the kinetics of absorption, the time required for each sample to reach 90% saturation was adopted as the criterion for assessing the absorption rate, based on the absorption profiles. The results at 25°C show that the blends of EDA+MEA and EDA+AMP demonstrated notable accelerated absorption rates, surpassing the benchmark pure EDA by 45% and 25%, respectively. In contrast, the blend containing the tertiary amine, EDA+MDEA, exhibited a similar absorption rate compared to pure EDA, with a deviation of 5% (Figure 3A). The absorption patterns observed at 50°C (Figure 3B) exhibited a similar trend to those at 25°C; however, the individual curves were more distinct at the lower temperature and reached saturation relatively sooner.

The absorption capacity measured by the change in the CO_2 loading (mol CO_2/mol amine) over time is presented at the top right corner of the figures (Figure 3A and Figure 3B). For each sample, the CO_2 loading gradually increased as CO_2 is absorbed, eventually reaching a plateau, which indicated the point of maximum CO_2 loading or saturated CO_2 loading at the end of the experiment. Contrary to the absorption kinetics, the absorption capacity demonstrated an opposite trend – the blend of EDA+MDEA showed the highest capacity for CO_2 absorption, surpassing the pure EDA by 20%. Other blends, EDA+AMP, and EDA+MEA, demonstrated lower CO_2 loading compared to pure EDA, with reductions of 7% and 17%, respectively. Similar to the absorption kinetics, the CO_2 loading trend for all the samples remained consistent at both temperatures. At the lower temperature of 25°C, the individual curves exhibited greater differentiation between the samples compared to the CO_2 loading curves at 50°C.

The trends in absorption kinetics and absorption capacity could be explained by the type of amine mixed with the EDA in each sample. The faster absorption kinetics of the EDA+MEA blend could be explained by the rapid reactions of the primary amine with CO_2, leading to the formation of carbamates. However, its limited theoretical CO_2 absorption capacity of only 0.5 moles of CO_2 per mole of amine [52, 53] is the lowest compared with the other samples. In contrast, the EDA+MDEA blend, containing the tertiary amine MDEA, did not engage in a direct reaction with CO_2, rather it produced bicarbonate and protonated amine species. This hydrolytic reaction is kinetically slower compared to the direct carbamate-forming reactions observed with MEA [54]. However, the EDA+MDEA blend possesses an advantage in terms of absorption capacity, as it can absorb more CO_2 because of the higher theoretical CO_2 loading of its constituent amine, MDEA; 1 mole of CO_2 per mole of amine [54, 55]. The sample containing the sterically hindered amine, EDA+AMP, was also found to react with CO_2 directly [11, 56], leading to the formation of carbamates, similar to MEA. However, the carbamate generated in the CO_2-AMP reaction is inherently unstable due to the chemical structure of AMP. Consequently, the unstable carbamate yielded bicarbonates and free AMP. This could explain why the CO_2 absorption capacity of EDA+AMP was observed to be slightly lower than the pure EDA which is a primary diamine having two amine groups, but it is notably higher than that of EDA+MEA.

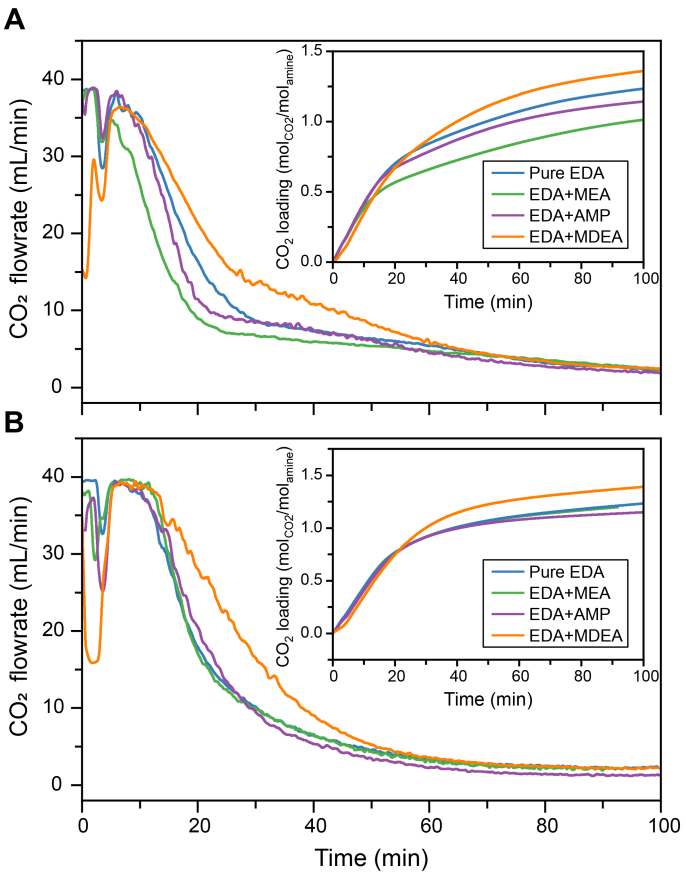

Figure 3. CO_2 absorption profiles and the corresponding CO_2 loading. The unsaturated samples were purged for 100 minutes with a simulated flue gas while the rate of the unabsorbed CO_2 coming out from the gas-tight absorption setup was measured. The absorption experiments were conducted at different temperatures of (A) 25°C and (B) 50°C. The total amine concentration in each sample was kept at 1 M. The CO_2 loading profiles (mol_{CO2}/mol_{amine}) over time are presented as an inset at each temperature.

In conventional amine-based CCS, when lean amine solution (low CO_2 loading) reacts with CO_2 in the absorber, the exothermic nature of the reaction releases a significant amount of energy which raises the solution temperature from 40°C to ~70°C. This phenomenon is commonly reported as a temperature bulge and necessitates further efforts to cool down the temperature in order to increase the absorption [57, 58]. A similar phenomenon was noticed in both temperatures; a sudden drop in CO_2 absorption for all samples, evidenced by the reduction in absorbed CO_2 flow rate within the first 10 minutes of the absorption experiment (Figure 3). The observed reduction in absorbed CO_2 flow rate during this early stage can be attributed to the significant heat of absorption when fresh lean amine solution is available for CO_2 to react. We further traced the temperature profiles of the sample to observe the possible connection between absorption decay and the temperature rise. Further analysis on the heat of absorption related to the individual samples was not performed in this study, however, the observed synchronized temperature raised during the early stages of absorption confirmed the established connection between the heat of absorption and absorption decay, as reported in the literature.

3.2 Physicochemical Properties of the Electrolyte

Previous research on EMAR focused solely on pure EDA as an electrolyte. Therefore, it is essential to measure the physicochemical properties of EDA blend electrolytes to confirm that no significant design alterations are needed in the overall EMAR process. These physicochemical properties included pH, ionic conductivity, viscosity, and FTIR measurements, before and after the saturation with CO_2. The measurement of pH serves as an initial indicator of the saturation, as CO_2, being an acidic gas, tends to reduce the pH of the amine solution. In all four samples, the initial pH was approximately 12, subsequently decreasing to approach a pH of 7 after 100 minutes of absorption to get fully saturated. The uniformity of the pH drops in all the samples at both temperatures, 25°C and 50°C (as illustrated in Figure 4A), indicates a consistent impact of the saturation process on the solution pH, irrespective of the particular composition of the amine blend.

In contrast to the pH change of the samples, an increase in the ionic conductivity of the electrolytes was observed (Figure 4B). This can be attributed to the introduction of carbamate or bicarbonates upon saturation, both of which contribute additional ions, thereby increasing the availability of charged species that positively impact ionic conductivity. Furthermore, the influence of temperature on ionic conductivities of the solutions was more pronounced compared to the temperature impact on the pH. Higher temperatures were found to result in increased ionic conductivities due to the increased mobility of charged species, subsequently leading to increased

conductivities [19, 59]. Similar to the pH change, the difference in conductivity (before and after the saturation) remained consistent across all the samples, indicating that the saturation process itself exerts a uniform effect on ionic conductivities, regardless of the specific composition of the amines in the blend.

The viscosity of the samples was measured before and after the saturation, across a broad temperature range from 25°C to 75°C (Figure 5C). This temperature range was chosen to gain a thorough understanding of the temperature's influence on the viscosity of the samples. Similar to the pH and ionic conductivity observations, there were no significant differences in the viscosities of the individual samples, whether they consisted of pure EDA or its blend with the secondary amines, at any of the tested temperatures. However, on average, the viscosity of the samples increased by approximately 9% after saturation, which can be attributed to the presence of carbamates and bicarbonates in the saturated samples. A consistent trend of decreasing viscosity as temperature increased was observed which aligns with prior studies conducted on CO_2 absorption in amine solutions and their temperature-dependent viscosity behavior [19, 60].

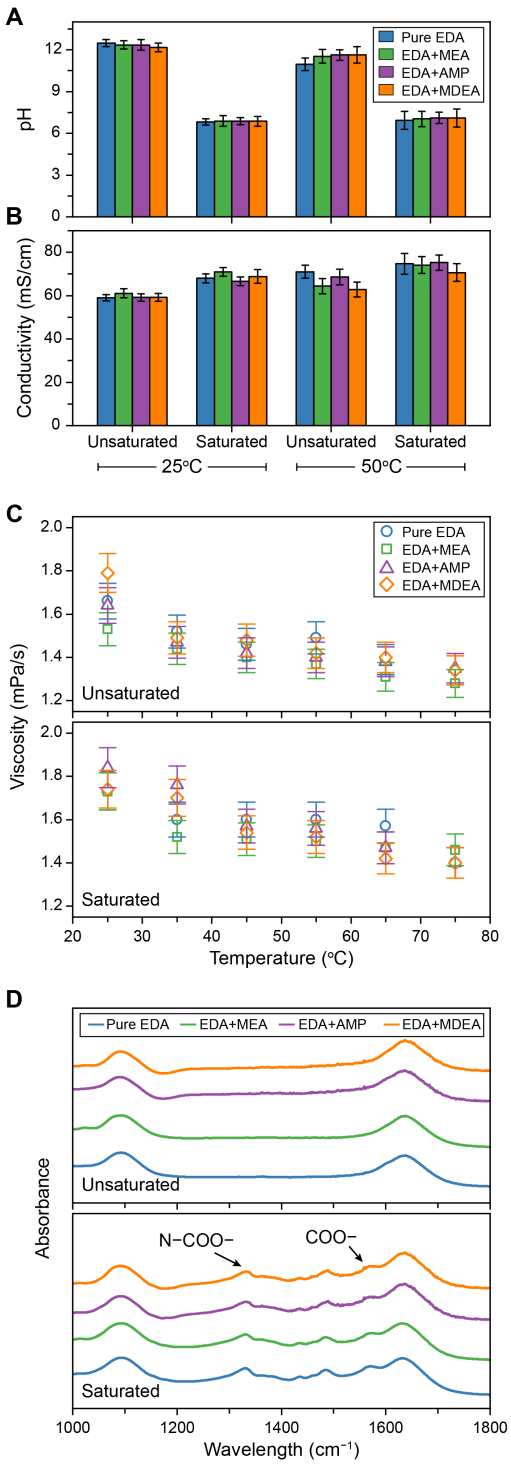

Figure 4. The physicochemical properties of electrolyte samples. The properties were measured for unsaturated and saturated samples: A) electrolytes pH and (B) ionic conductivity at two temperatures of 25°C and 50°C; (C) viscosity at temperatures ranging from 25°C to 75°C; and (D) absorbance spectra of the electrolytes obtained from FTIR measurements. Error bars represent the standard errors.

The observed results, including a drop in pH and an increase in ionic conductivity as well as enhanced viscosity after CO_2 saturation, all correspond to the introduction of carbamate and bicarbonate. To confirm the presence of these species upon saturation, FTIR measurements were conducted on samples both before and after saturation. The emergence of new peaks for saturated samples compared to the unsaturated samples, specifically in the range of 1200 cm^{-1} to 1600 cm^{-1} wavelength, confirmed the formation of carbamate and bicarbonate-related functional groups (Figure 4D). These peaks correspond to specific vibrational modes associated with the asymmetric stretching of the COO− group and the stretching of the N−COO− bond linked with the presence of carbamate and bicarbonate species [61, 62]. Overall, the physicochemical properties of the blend electrolytes showed no significant differences compared to the benchmark EDA electrolyte. This confirms that no major modifications are needed in the EMAR process scheme, configuration, and components.

3.3 Desorption Kinetics

The kinetics of CO_2 desorption were compared between the blend electrolytes and the benchmark EDA sample by injecting cupric ions (Cu^{2+}) into the saturated solutions. Theoretically, each mole of Cu^{2+} leads to the desorption of two moles of CO_2, as it competitively bonds with the saturated electroactive amine, i.e., EDA, thereby releasing CO_2. The supply of Cu^{2+} to the saturated samples simulates the electrochemical reaction where the oxidation of the active Cu anode provides the Cu^{2+} to the bulk electrolyte, resulting in the desorption of CO_2 ($Cu \rightarrow Cu^{2+} + 2\ e^-$ followed by $Cu^{2+} + 2$ amine-$CO_2 \rightarrow Cu(amine)_2^{2+} + 2\ CO_2$). The introduction of Cu^{2+} to the electrolyte results in increasing copper loading (mol Cu/mol of amine) over time. The desorption experiments were performed for all the samples at two different temperatures (Figure 5). The blend samples release CO_2 and reach a plateau (indicating full desorption) significantly faster at both temperatures. The presence of the secondary amines with the EDA possibly assisted the desorption process compared to the pure EDA sample which takes more time (indicative of copper loading) to desorb fully. This promoting effect can likely be attributed to three phenomena: 1) the partial complexation of the secondary amine with Cu^{2+}, which aids in desorbing CO_2 not only from the electroactive amine, EDA, but also from the secondary amine; 2) the presence of secondary amine to shift the bicarbonate equilibrium toward CO_2 formation; and 3) the impact of secondary amines on the intermediate species in the desorption process, enhancing their kinetic factors. To quantify the extent of desorption, the samples at the end of the desorption experiment were acid-titrated to measure the CO_2 loading. The pure EDA sample, consisting of 100% electroactive amine, desorbed the most CO_2 compared to the blends of the samples that only have 80% of the

electroactive content. However, all the blend samples desorbed more than 80% of CO_2 upon increasing the copper loading (Figure 5C), thus meeting the desorption requirement for an efficient EMAR cycle [31]. At 50°C, all samples, regardless of their composition, released more CO_2 compared to 25°C, likely due to the additional thermal force at elevated temperatures that facilitates CO_2 desorption by partial thermal swing from the solution.

3.4 Electrochemical Characterizations

Detailed electrochemical measurements, including EIS and RDE, were conducted to elucidate the influence of different blend amines on redox reactions. The EIS technique was employed to quantify the changes in the individual components of the resistances and compare the pure EDA sample with the samples containing the blends of EDA. EIS measurements were conducted for both the cathode and anode. For the cathode, the WE was negatively polarized to investigate the deposition process, while for the anode, it was positively charged to study the corrosion process. For both deposition and corrosion processes, the R_{CT} values were significantly reduced when a blend amine was used compared to pure EDA. In deposition, the largest drop of 79% was observed for the EDA+MDEA blend, followed by a 70% drop for EDA+AMP and EDA+MEA blends (Figure 6A). In corrosion, the largest drop of 62% was observed for the EDA+MDEA sample (Figure 6B).

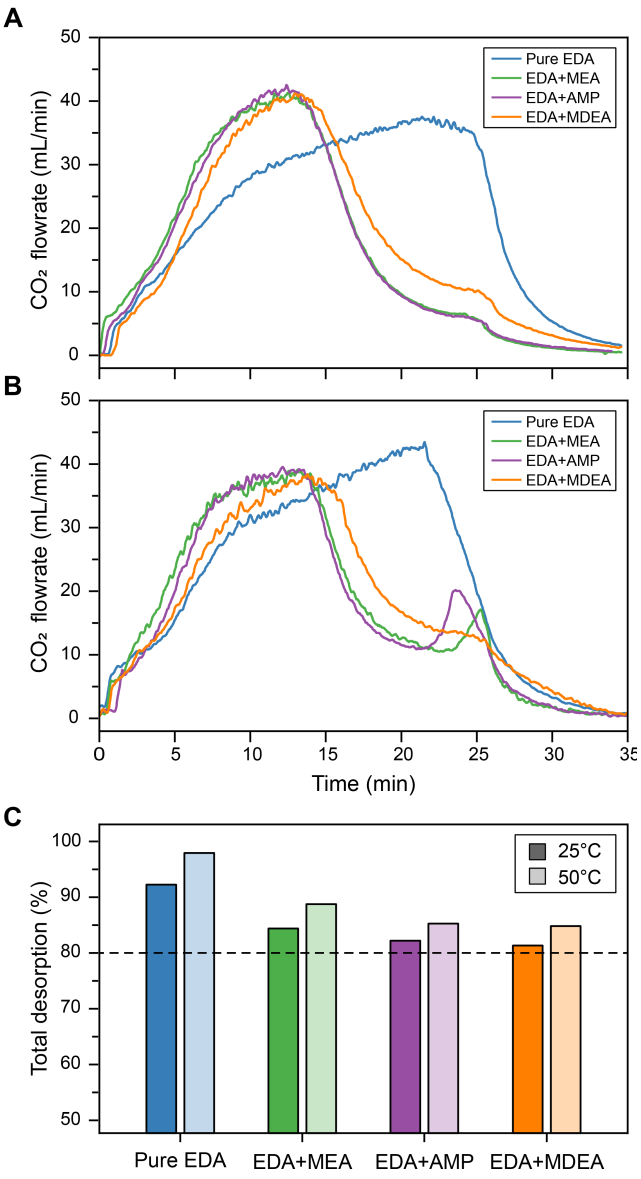

Figure 5. Desorption kinetics of the saturated samples. The desorption experiments were conducted by injecting cupric ions (Cu^{2+}) and the desorbed CO_2 flowrates were recorded. The desorption experiments were conducted at two different temperatures of A) 25°C and B) 50°C. (C) The total percentage of CO_2 desorbed relative to the absorbed level was also measured at both temperatures using the titration method. The dashed line indicates the target total desorption.

In contrast to R_{CT}, the R_S values were consistent across all samples in both deposition and corrosion processes, with a deviation of less than 10% observed among different solution types. Given that R_S is directly related to solution conductivity, and since similar conductivity ranges were observed for all samples (see Figure 4B), this consistency in R_S values can be attributed to the uniform conductivity across the samples.

When comparing R_{CT} and R_S, it is evident that R_{CT} contributes more significantly to the total resistance in almost all samples (Figure 6C). Comparing the deposition and corrosion processes, the total resistance towards deposition was substantially higher than that for corrosion, irrespective of the solution type. This indicates that the overall redox process is predominantly limited by the deposition step. A similar trend was observed in another EMAR process when assessing the impact of supporting electrolytes using the Tafel technique [31]. Among all the solutions, the EDA+ MDEA sample exhibited the lowest total resistance. The resistance values are summarized in Table 1 for all samples, including both deposition and corrosion processes.

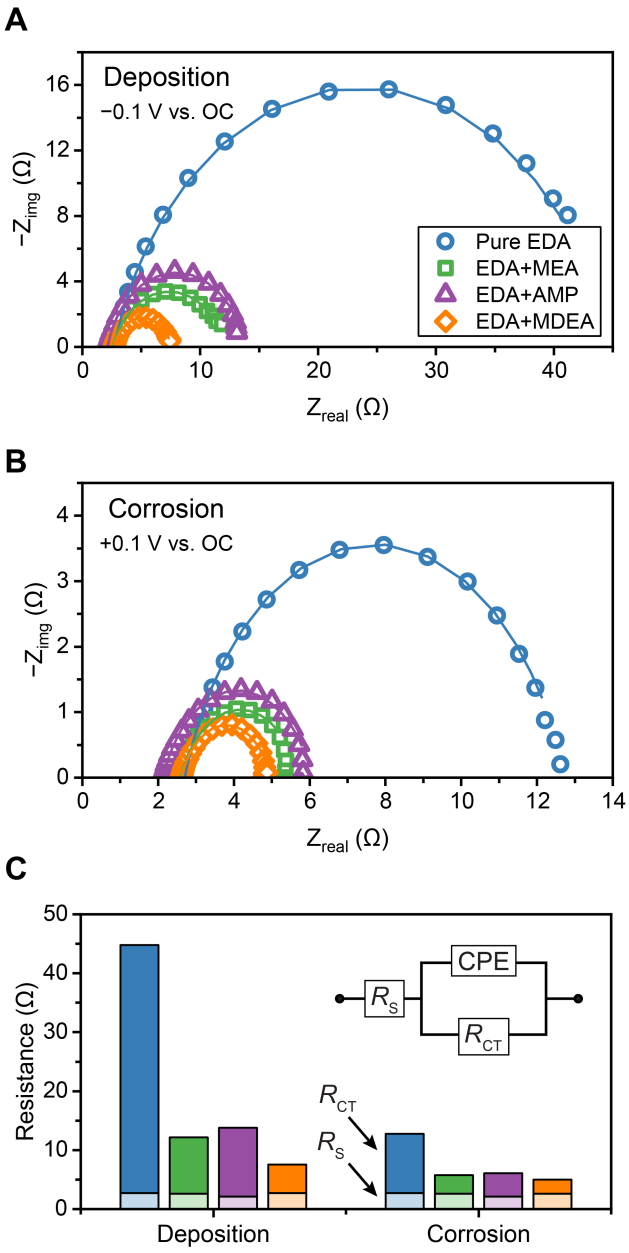

Figure 6. Resistance analysis using the EIS technique. Nyquist plot representation of the EIS data when the working electrode (WE) was polarized as (A) a negative electrode at −0.1 V vs. open circuit (OC) to perform the deposition process, and (B) a positive electrode at 0.1 V vs. OC to facilitate the corrosion process; (C) A Randles equivalent circuit with a constant phase element (CPE) was used to fit the EIS data to reveal the components of the total resistance, including the solution resistance (R_S) and the charge transfer resistance (R_{CT}) for all the electrolyte solution with a total amine concentration of 1 M. The symbols in panels A and B represent the EIS data, while the lines indicate the fitted model based on the equivalent Randles circuit.

Table 1. Solution resistance (R_S) and charge transfer resistance (R_{CT}) values calculated from the Nyquist plot for the deposition and corrosion reactions during the EIS measurements.

Sample	Deposition			Corrosion		
	R_S (Ω)	R_{CT} (Ω)	Total (Ω)	R_S (Ω)	R_{CT} (Ω)	Total (Ω)
EDA	2.71	42.11	44.82	2.70	10.04	12.74
EDA+MEA	2.60	9.53	12.13	2.60	3.15	5.75
EDA+AMP	2.13	11.66	13.79	2.12	3.95	6.07
EDA+MDEA	2.70	4.86	7.56	2.61	2.36	4.97

Deposition, identified as the rate-limiting step, was further investigated using the RDE technique. By employing RDE, the effects of mass transport are negated, allowing for a detailed investigation into the kinetic aspects of the process. Levich experiments were conducted for all samples, providing insights into the heterogeneous electron transfer rate constant (k^0), a key indicator of the reaction kinetics in the deposition process. The Levich experiment results reveal that the EDA+MDEA blend exhibits the highest k^0 (4.15 x 10^{-6} cm/s) compared to other blends and pure EDA (1.37 x 10^{-6} cm/s; Figure 7). This aligns with the R_{CT} findings from the EIS experiments, confirming that the presence of MDEA in the electrolyte results in the fastest electrochemical kinetics in the deposition reaction.

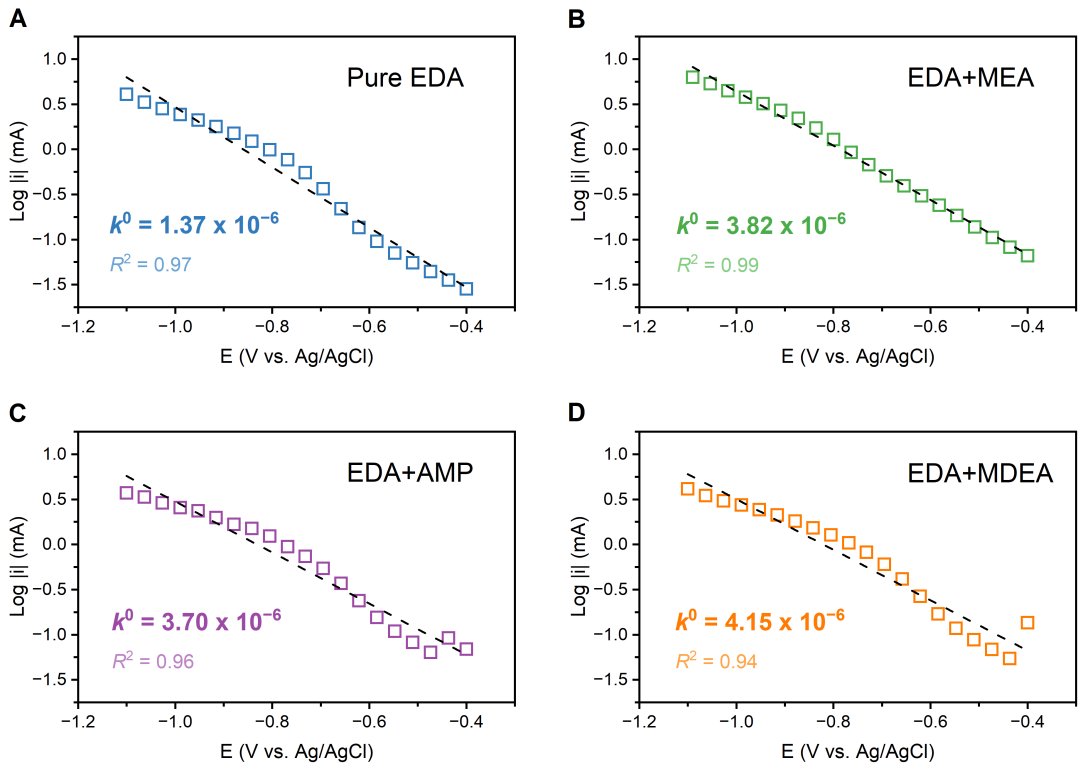

Figure 7. Heterogenous reaction rate constant estimation by Levich Analysis. The experiments were performed using a rotating disk electrode (RDE) by rotating the working electrode (WE) at different speeds while sweeping the voltage. The values of the cathodic current in the Tafel region were taken to perform the Levich analysis for the estimation of the heterogeneous electron transfer reaction rate constants (k^0) for the samples (A) Pure EDA, (B) EDA+MEA, (C) EDA+AMP, and (D) EDA+MDEA. The R-squared (R^2) values represent the fitting quality of the linear model.

3.5 Selection of High-Performance Amine Blend

The results from absorption, desorption, and electrochemical measurements were combined to identify an amine blend to be utilized in the bench-scale demonstration, aimed at improving the performance of the EMAR process (Figure 8). Generally, the tested blend amines showed superior performance compared to the benchmark pure EDA across all three categories. Among the investigated samples, the EDA+MDEA blend stood out, particularly in the electrochemical tests. While this blend exhibited lower absorption kinetics, this limitation can be effectively addressed by incorporating rate promoters, which is a common practice in conventional amine-based carbon capture processes [63, 64]. Therefore, the blend of EDA+MDEA was selected for further investigation in the bench-scale process to assess the energetics of carbon capture and to draw a comparison with the benchmark EDA-based EMAR process.

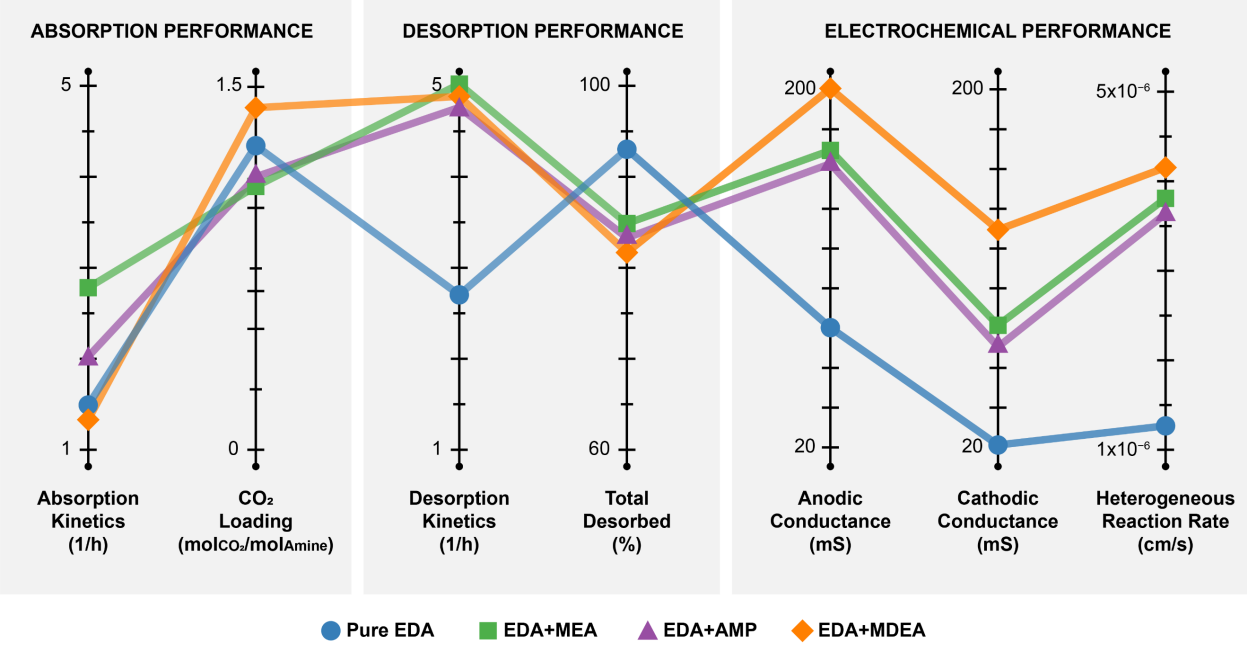

Figure 8. A quantitative comparison of the performance of different amine blends. A summary presenting the absorption and desorption performance, including kinetics, capacity, and total desorbed CO_2, alongside the electrochemical performance including the conductance values (i.e., the reverse of the total resistance) and heterogeneous electron transfer reaction rate constant for all samples.

3.6 Bench Scale Performance

A bench scale performance of an EMAR process operated with either pure EDA or the EDA+MDEA blend was investigated following the protocol described earlier. Figure 9 illustrates the voltage response of a chronopotentiometry experiment performed by applying 0.5 A current for 80 minutes. For both samples, the voltage initially increased at the beginning of the experiment and reached a stable value before rising again. The sudden rise in voltage at the start of the

reaction can be attributed to the availability of electroactive species near the electrode. The electrochemical reaction quickly drew the voltage to facilitate the reaction. Once the reaction reached a stable point where there was a continuous and uniform supply of reactants, the voltage remained stable. However, the electroactive species were consumed towards the end of the experiment, and their concentration decreased, leading to a rise in voltage.

It was observed that the pure EDA required a higher voltage to drive the same current compared to the EDA+MDEA blend (Figure 9A). This can be attributed to the lower R_{CT} and higher k^0 observed for the blend sample compared to pure EDA. The higher required voltage potentially resulted in a higher absolute energy requirement to drive the process for the pure EDA sample. However, to assess the normalized energetics (i.e., the energy required to desorb 1 mole of CO_2), the rate of CO_2 desorption must also be taken into account. Therefore, the CO_2 output flows for both the EDA+MDEA blend and pure EDA samples were carefully monitored. The results show that the average CO_2 desorption rate for the EDA+MDEA blend was slightly higher than that of pure EDA (Figure 9B).

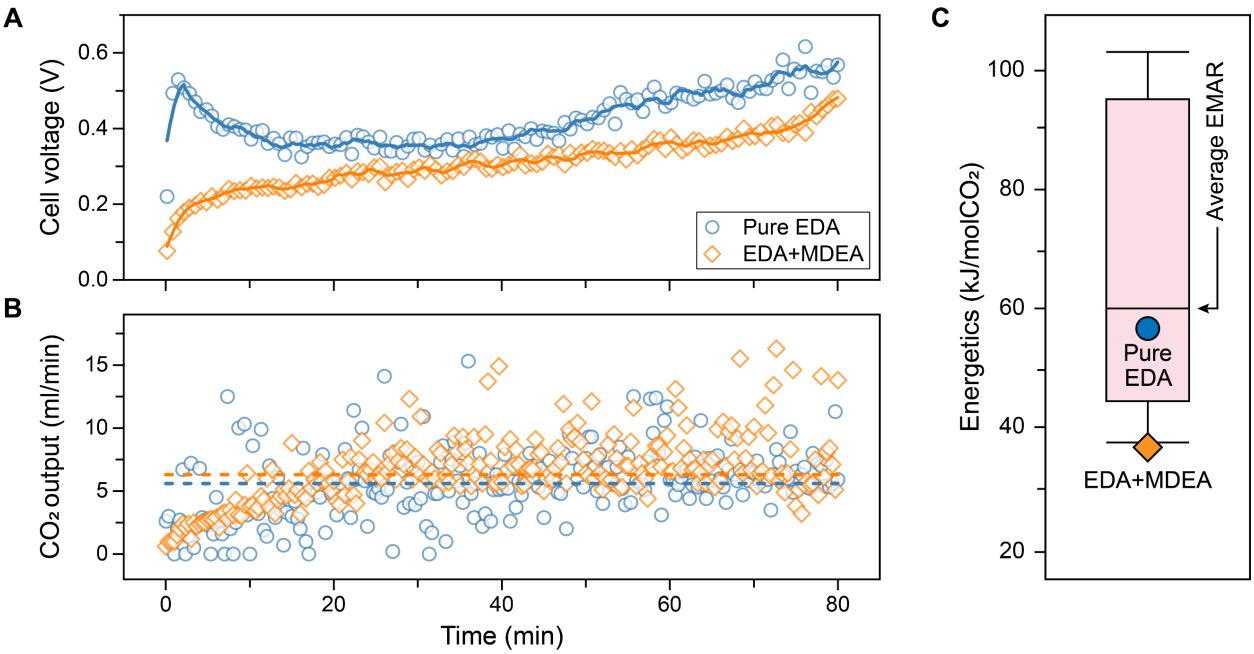

Figure 9. Bench scale performance of the EMAR cell with the optimized amine blend. Chronopotentiometry was performed on statured samples of pure EDA and EDA+MDEA blend by applying a fixed 0.5 A current for 80 minutes: (A) the voltage response was monitored along with (B) the desorbed gas flowrate. The symbols represent the actual voltage and CO_2 output data taken. The solid lines in panel A represent the smoothed voltage profiles, while the dashed lines in panel B represent the average values of the desorption rate for each sample. (C) The energetics of EMAR operating with both pure EDA and EDA+MDEA samples were calculated (symbols) and compared to the values reported in the literature for other EMAR processes developed for point source carbon capture (represented in the whisker diagram).

Taking into account both the required potential and the CO_2 desorption rate, the normalized energetics of the EMAR process were calculated for the EDA+MDEA blend and pure EDA. The results demonstrated significantly lower energetics for the blend (37 kJ/molCO_2) compared to pure EDA (56 kJ/molCO_2), confirming the superior performance of the newly developed electrolyte over the benchmark EDA solution. Furthermore, these energetics were compared with other EMAR processes used for carbon capture from industrial flue gas. Notably, the energetics of the blend absorbent developed in this study was the lowest yet reported for an EMAR process. This new blend resulted in an approximate 40% reduction in the energy requirement for carbon capture relative to the average values reported for EMAR processes (Figure 9C). This substantial performance gain is primarily attributed to the facilitation of the rate-limiting deposition process.

4 CONCLUSIONS

In this investigation, for the first time, the absorbent chemistry of the EMAR process was revived by considering criteria beyond metal ion complexation. The use of secondary amines, previously overlooked due to their limited interaction with metal ions but known for their high performance in conventional carbon capture processes, was systematically investigated. The study comprehensively examined the addition of secondary amines (MEA, AMP, and MDEA) to the benchmark EDA, assessing their absorption and desorption kinetics and capacities, along with their electrochemical performance. Among the blends, EDA+MDEA emerged as the top performer, particularly excelling in electrochemical aspects. The charge transfer resistance for the EDA+MDEA blend was reduced by 40% compared to pure EDA, and the heterogeneous electron transfer rate constant improved threefold. In the bench-scale experiments, the EDA+MDEA blend showed a notable decrease in desorption energetics to 37 kJ/molCO_2, marking a 34% reduction compared to the 56 kJ/molCO_2 required for pure EDA. This achievement marks the lowest energetics reported for an EMAR process aimed at point source carbon capture.

Looking ahead, the optimized EDA+MDEA blend presents an opportunity for further enhancement by incorporating a rate promoter during the absorption stage. Future studies could explore various rate promoters, such as amino acids, commonly used in conventional tertiary amine-based carbon capture processes. Assessing the impact of these promoters on the blend's electrochemical performance will be crucial. Moreover, this study's experimental design and outcomes lay the groundwork for broader investigations into a more extensive range of amine blends for EMAR. While this research focused on three specific secondary amines, future work could extend to a

diverse array of amines previously used in traditional amine-based carbon capture. Additionally, long-term operation assessments to evaluate electrolyte and electrode stability and durability would be a valuable direction for subsequent research. This multi-faceted approach promises to further refine and expand the potential of EMAR technologies in carbon capture applications.

ACKNOWLEDGMENTS

The authors acknowledge the support from the Center for Carbon Management in Energy (CCME) of UH Energy, through seed funding (Award Number: G0509373). Additionally, we acknowledge the University of Houston's Division of Research for the new faculty startup package granted to Dr. Rahimi.

REFERENCES

1. Rogelj, J., M. den Elzen, N. Höhne, T. Fransen, H. Fekete, H. Winkler, R. Schaeffer, F. Sha, K. Riahi, and M. Meinshausen, *Paris Agreement climate proposals need a boost to keep warming well below 2 °C.* Nature, 2016. **534**(7609): p. 631-639.
2. Intergovernmental Panel on Climate, C., *Climate Change 2021 – The Physical Science Basis: Working Group I Contribution to the Sixth Assessment Report of the Intergovernmental Panel on Climate Change*. 2023, Cambridge: Cambridge University Press.
3. Rahimi, M., A. Khurram, T.A. Hatton, and B. Gallant, *Electrochemical carbon capture processes for mitigation of CO2 emissions.* Chemical Society Reviews, 2022. **51**(20): p. 8676-8695.
4. Rahimi, M., *Public awareness: What climate change scientists should consider.* Sustainability, 2020. **12**(20): p. 8369.
5. Johnsson, F., J. Kjärstad, and J. Rootzén, *The threat to climate change mitigation posed by the abundance of fossil fuels.* Climate Policy, 2019. **19**(2): p. 258-274.
6. Martin-Roberts, E., V. Scott, S. Flude, G. Johnson, R.S. Haszeldine, and S. Gilfillan, *Carbon capture and storage at the end of a lost decade.* One Earth, 2021. **4**(11): p. 1569-1584.
7. Rochelle, G.T., *Amine Scrubbing for CO2 Capture.* Science, 2009. **325**(5948): p. 1652-1654.
8. Liang, Z., W. Rongwong, and H. Liu, *Recent progress and new developments in post-combustion carbon-capture technology with amine based solvents.* International Journal of Greenhouse Gas Control, 2o15.
9. Rahimi, M., S.M. Moosavi, B. Smit, and T.A. Hatton, *Toward smart carbon capture with machine learning.* Cell Reports Physical Science, 2021. **2**(4): p. 100396.
10. Wu, Y., J. Xu, K. Mumford, G.W. Stevens, W. Fei, and Y. Wang, *Recent advances in carbon dioxide capture and utilization with amines and ionic liquids.* Green Chemical Engineering, 2020. **1**(1): p. 16-32.

11. Chen, M., H. Gao, T. Sema, M. Xiao, Q. Sun, and Z. Liang, *Study on the mechanism and kinetics of amine with steric hindrance absorbing CO2 in non-aqueous/aqueous solution.* Separation and Purification Technology, 2022. **303**: p. 122202.

12. Mao, Y., X. Yang, and T.V. Gerven, *Amine-Assisted Simultaneous CO2 Absorption and Mineral Carbonation: Effect of Different Categories of Amines.* Environmental Science & Technology, 2023. **57**(29): p. 10816-10827.

13. Donaldson, T.L. and Y.N. Nguyen, *Carbon Dioxide Reaction Kinetics and Transport in Aqueous Amine Membranes.* Industrial & Engineering Chemistry Fundamentals, 1980. **19**(3): p. 260-266.

14. IEA, *Environmental impacts of amine emissions during post combustion capture*. 2010.

15. Rochelle, G.T., *Thermal degradation of amines for CO2 capture.* Current Opinion in Chemical Engineering, 2012. **1**(2): p. 183-190.

16. Park, J., S. Yoon, S.-Y. Oh, Y. Kim, and J.-K. Kim, *Improving energy efficiency for a low-temperature CO2 separation process in natural gas processing.* Energy, 2021. **214**: p. 118844.

17. Aleta, P., A. Refaie, M. Afshari, A. Hassan, and M. Rahimi, *Direct ocean capture: the emergence of electrochemical processes for oceanic carbon removal.* Energy & Environmental Science, 2023. **16**: p. 4944-4967.

18. Sharifian, R., R.M. Wagterveld, I.A. Digdaya, C. Xiang, and D.A. Vermaas, *Electrochemical carbon dioxide capture to close the carbon cycle.* Energy & Environmental Science, 2021. **14**(2): p. 781-814.

19. Rahimi, M., K.M. Diederichsen, N. Ozbek, M. Wang, W. Choi, and T.A. Hatton, *An Electrochemically Mediated Amine Regeneration Process with a Mixed Absorbent for Postcombustion CO2 Capture.* Environmental Science & Technology, 2020. **54**(14): p. 8999-9007.

20. Stern, M.C. and T.A. Hatton, *Bench-scale demonstration of CO2 capture with electrochemically-mediated amine regeneration.* RSC Advances, 2014. **4**(12): p. 5906-5914.

21. Simeon, F., M.C. Stern, K.M. Diederichsen, Y. Liu, H.J. Herzog, and T.A. Hatton, *Electrochemical and molecular assessment of quinones as co2-binding redox molecules for carbon capture.* The Journal of Physical Chemistry C, 2022. **126**(3): p. 1389-1399.

22. Voskian, S. and T.A. Hatton, *Faradaic electro-swing reactive adsorption for CO2 capture.* Energy & Environmental Science, 2019. **12**(12): p. 3530-3547.

23. Barlow, J.M. and J.Y. Yang, *Oxygen-stable electrochemical CO2 capture and concentration with quinones using alcohol additives.* Journal of the American Chemical Society, 2022. **144**(31): p. 14161-14169.

24. Jin, S., M. Wu, R.G. Gordon, M.J. Aziz, and D.G. Kwabi, *pH swing cycle for CO2 capture electrochemically driven through proton-coupled electron transfer.* Energy & Environmental Science, 2020. **13**(10): p. 3706-3722.

25. Rahimi, M., G. Catalini, S. Hariharan, M. Wang, M. Puccini, and T.A. Hatton, *Carbon Dioxide Capture Using an Electrochemically Driven Proton Concentration Process.* Cell Reports Physical Science, 2020. **1**(4): p. 100033.

26. Rahimi, M., G. Catalini, M. Puccini, and T.A. Hatton, *Bench-scale demonstration of CO2 capture with an electrochemically driven proton concentration process.* RSC advances, 2020. **10**(29): p. 16832-16843.

27. Jin, S., M. Wu, Y. Jing, R.G. Gordon, and M.J. Aziz, *Low energy carbon capture via electrochemically induced pH swing with electrochemical rebalancing.* Nature Communications, 2022. **13**(1): p. 2140.

28. Bilal, M., J. Li, H. Guo, and K. Landskron, *High-Voltage Supercapacitive Swing Adsorption of Carbon Dioxide.* Small, 2023. **19**(24): p. 2207834.

29. Bilal, M., J. Li, and K. Landskron, *Enhancing Supercapacitive Swing Adsorption of CO2 with Advanced Activated Carbon Electrodes.* Advanced Sustainable Systems, 2023: p. 2300250.

30. Legrand, L., O. Schaetzle, R. De Kler, and H. Hamelers, *Solvent-free CO2 capture using membrane capacitive deionization.* Environmental science & technology, 2018. **52**(16): p. 9478-9485.

31. Wang, M., S. Hariharan, R.A. Shaw, and T.A. Hatton, *Energetics of electrochemically mediated amine regeneration process for flue gas CO2 capture.* International Journal of Greenhouse Gas Control, 2019. **82**: p. 48-58.

32. Hasanzadeh, A., S.G. Holagh, M. Janbazvatan, H. Rashidpour, A. Chitsaz, and M. Khalilian, *Electrochemically mediated amine regeneration and proton concentration modulation processes for flue gas CO2 capture: Comparison and artificial intelligence-based optimization.* Journal of CO2 Utilization, 2023. **67**: p. 102306.

33. Kuo, F.-Y., S.E. Jerng, and B.M. Gallant, *Dual Salt Cation-Swing Process for Electrochemical CO2 Separation.* ACS Central Science, 2023. **9**(9): p. 1750-1757.

34. Khurram, A., M. He, and B.M. Gallant, *Tailoring the discharge reaction in Li-CO2 batteries through incorporation of CO2 capture chemistry.* Joule, 2018. **2**(12): p. 2649-2666.

35. Boualavong, J. and C.A. Gorski, *Electrochemically Mediated CO2 Capture Using Aqueous Cu (II)/Cu (I) Imidazole Complexes.* ACS ES&T Engineering, 2021. **1**(7): p. 1084-1093.

36. Liu, Y., H.-Z. Ye, K.M. Diederichsen, T. Van Voorhis, and T.A. Hatton, *Electrochemically mediated carbon dioxide separation with quinone chemistry in salt-concentrated aqueous media.* Nature Communications, 2020. **11**(1): p. 2278.

37. Rahimi, M., F. Zucchelli, M. Puccini, and T. Alan Hatton, *Improved CO2 Capture Performance of Electrochemically Mediated Amine Regeneration Processes with Ionic Surfactant Additives.* ACS Applied Energy Materials, 2020. **3**(11): p. 10823-10830.

38. Wu, X., Y. Mao, H. Fan, S. Sultan, Y. Yu, and Z. Zhang, *Investigation on the performance of EDA-based blended solvents for electrochemically mediated CO2 capture.* Applied Energy, 2023. **349**: p. 121656.

39. Fan, H., Y. Mao, J. Gao, S. Tong, Y. Yu, X. Wu, and Z. Zhang, *Combined experimental and computational study for the electrode process of electrochemically mediated amine regeneration (EMAR) CO2 capture.* Applied Energy, 2023. **350**: p. 121771.

40. Wu, X., H. Fan, M. Sharif, Y. Yu, K. Wei, Z. Zhang, and G. Liu, *Electrochemically-mediated amine regeneration of CO2 capture: From electrochemical mechanism to bench-scale visualization study.* Applied Energy, 2021. **302**: p. 117554.

41. Stern, M.C., F. Simeon, H. Herzog, and T.A. Hatton, *Post-combustion carbon dioxide capture using electrochemically mediated amine regeneration.* Energy & Environmental Science, 2013. **6**(8): p. 2505-2517.

42. Wang, M., M. Rahimi, A. Kumar, S. Hariharan, W. Choi, and T.A. Hatton, *Flue gas CO2 capture via electrochemically mediated amine regeneration: System design and performance.* Applied Energy, 2019. **255**: p. 113879.

43. Stern, M.C., *Electrochemically-mediated amine regeneration for carbon dioxide separations*. 2014, Massachusetts Institute of Technology.

44. Wang, M., *Flue gas CO_2 capture using electrochemically mediated amine regeneration*, in *Department of Chemical Engineering*. 2020, Massachusetts Institute of Technology.

45. Wang, M., H.J. Herzog, and T.A. Hatton, *CO2 Capture Using Electrochemically Mediated Amine Regeneration.* Industrial & Engineering Chemistry Research, 2020. **59**(15): p. 7087-7096.

46. Chen, G., G. Chen, M. Peruzzini, R. Zhang, and F. Barzagli, *Understanding the potential benefits of blended ternary amine systems for CO2 capture processes through 13C NMR speciation study and energy cost analysis.* Separation and Purification Technology, 2022. **291**: p. 120939.

47. Adeosun, A. and M.R.M. Abu-Zahra, *Evaluation of amine-blend solvent systems for CO2 post-combustion capture applications.* Energy Procedia, 2013. **37**: p. 211-218.

48. Zhou, X., G. Jing, B. Lv, F. Liu, and Z. Zhou, *Low-viscosity and efficient regeneration of carbon dioxide capture using a biphasic solvent regulated by 2-amino-2-methyl-1-propanol.* Applied Energy, 2019. **235**(C): p. 379-390.

49. Tan, Y., W. Nookuea, H. Li, E. Thorin, and J. Yan, *Property impacts on Carbon Capture and Storage (CCS) processes: A review.* Energy Conversion and Management, 2016. **118**: p. 204-222.

50. Rahimi, M., A. D'Angelo, C.A. Gorski, O. Scialdone, and B.E. Logan, *Electrical power production from low-grade waste heat using a thermally regenerative ethylenediamine battery.* Journal of Power Sources, 2017. **351**: p. 45-50.

51. Rahimi, M., T. Kim, C.A. Gorski, and B.E. Logan, *A thermally regenerative ammonia battery with carbon-silver electrodes for converting low-grade waste heat to electricity.* Journal of Power Sources, 2018. **373**: p. 95-102.

52. Ma, C., F. Pietrucci, and W. Andreoni, *Capture and Release of CO2 in Monoethanolamine Aqueous Solutions: New Insights from First-Principles Reaction Dynamics.* Journal of Chemical Theory and Computation, 2015. **11**(7): p. 3189-3198.

53. Lv, B., B. Guo, Z. Zhou, and G. Jing, *Mechanisms of CO2 Capture into Monoethanolamine Solution with Different CO2 Loading during the Absorption/Desorption Processes.* Environmental Science & Technology, 2015. **49**(17): p. 10728-10735.

54. Idem, R., M. Wilson, P. Tontiwachwuthikul, A. Chakma, A. Veawab, A. Aroonwilas, and D. Gelowitz, *Pilot Plant Studies of the CO2 Capture Performance of Aqueous MEA and Mixed MEA/MDEA Solvents at the University of Regina CO2 Capture Technology Development Plant and the Boundary Dam CO2 Capture Demonstration Plant.* Industrial & Engineering Chemistry Research, 2006. **45**(8): p. 2414-2420.

55. Aroonwilas, A. and A. Veawab, *Characterization and Comparison of the CO2 Absorption Performance into Single and Blended Alkanolamines in a Packed Column.* Industrial & Engineering Chemistry Research, 2004. **43**(9): p. 2228-2237.

56. Kang, M.-K., I.-D. Kim, B.-J. Kim, J.-S. Kang, and K.-J. Oh, *Characteristics of Absorption/Regeneration of AMP/MEA Using Hybrid Packing for the Improvement of CO2*

Absorption Performance. Industrial & Engineering Chemistry Research, 2015. **54**(22): p. 5853-5861.

57. Kvamsdal, H.M. and G.T. Rochelle, *Effects of the Temperature Bulge in CO2 Absorption from Flue Gas by Aqueous Monoethanolamine.* Industrial & Engineering Chemistry Research, 2008. **47**(3): p. 867-875.

58. Zheng, Y., E. El Ahmar, M. Simond, K. Ballerat-Busserolles, and P. Zhang, *CO2 Heat of Absorption in Aqueous Solutions of MDEA and MDEA/Piperazine.* Journal of Chemical & Engineering Data, 2020. **65**(8): p. 3784-3793.

59. Han, S.-J. and J.-H. Wee, *CO2 Absorption Performance and Electrical Properties of 2-Amino-2-methyl-1-propanol Compared to Monoethanolamine Solutions as Primary Amine-Based Absorbents.* Energy & Fuels, 2021. **35**(4): p. 3197-3207.

60. Kummamuru, N.B., D.A. Eimer, and Z. Idris, *Viscosity Measurement and Correlation of Unloaded and CO2-Loaded Aqueous Solutions of N-Methyldiethanolamine + 2-Amino-2-methyl-1-propanol.* Journal of Chemical & Engineering Data, 2020. **65**(6): p. 3072-3078.

61. Richner, G. and G. Puxty, *Assessing the Chemical Speciation during CO2 Absorption by Aqueous Amines Using in Situ FTIR.* Industrial & Engineering Chemistry Research, 2012. **51**(44): p. 14317-14324.

62. Jackson, P., K. Robinson, G. Puxty, and M. Attalla, *In situ Fourier Transform-Infrared (FT-IR) analysis of carbon dioxide absorption and desorption in amine solutions.* Energy Procedia, 2009. **1**(1): p. 985-994.

63. Richner, G., *Promoting CO2 absorption in aqueous amines with benzylamine.* Energy Procedia, 2013. **37**: p. 423-430.

64. Alivand, M.S., O. Mazaheri, Y. Wu, G.W. Stevens, C.A. Scholes, and K.A. Mumford, *Preparation of Nanoporous Carbonaceous Promoters for Enhanced CO2 Absorption in Tertiary Amines.* Engineering, 2020. **6**(12): p. 1381-1394.